https://doi.org/10.1016/j.nanoen.2023.108388
This is the Pre-Published Version.

Enhancing Water Droplet-based Electricity Generator by Harnessing Multiple-dielectric Layers Structure

Kaiqiang Wang[1,2], Wanghuai Xu[2], Jianfeng Li[1], Huanxi Zheng[2], Shouyi Sun[1,3], Wei Song[1], Yuxin Song[4], Zhengmao Ding[1], Rui Zhang[1], Yilin Sun[5], Hanli Zhang[1], Jinjin Li[1*] and Zuankai Wang[2*]

[1] State Key Laboratory of Tribology in Advanced Equipment, Tsinghua University, Beijing, 100084, China.

[2] Department of Mechanical Engineering, The Hong Kong Polytechnic University, Hong Kong, 999077, China.

[3] Department of Engineering Mechanics, Northwestern Polytechnical University (Chang'an Campus), 710129, China

[4] Department of Mechanical Engineering, City University of Hong Kong, Hong Kong, 999077, China.

[5] School of Vehicle and Mobility, Tsinghua University, Beijing, 100084, China.

*** Corresponding authors:**

Jinjin Li (E-mail: lijinjin@mail.tsinghua.edu.cn)

Zuankai Wang (E-mail: zk.wang@polyu.edu.hk)

© 2023. This manuscript version is made available under the CC-BY-NC-ND 4.0 license https://creativecommons.org/licenses/by-nc-nd/4.0/

Abstract

Harvesting water energy is promising to relieve the global energy crisis and reach the aim of carbon neutrality. However, few effective technologies can make use of water droplets as a power source efficiently. The droplet-based electricity generator (DEG) with a transistor-inspired design has resulted in enhanced energy harvesting efficiency by orders of magnitude over traditional designs. Despite this, the current DEG generally features a single dielectric layer, limiting its integration with other common objects to achieve "unnoticed" energy harvesting. In this work, we report a novel design featuring multiple dielectric layers-based DEG (M-DEG) that leverages other materials, such as household glass or umbrellas, as the second dielectric layer under the surface triboelectric layer to harvest water droplet energy without interfering with the original function of both. We find that the second dielectric layer enhances the output of M-DEG because of higher equivalent capacitance and charge density. The open circuit voltage and short-circuit current are increased by 90.6% and 68.7%, respectively. The maximal short-circuit current reaches up to record-breaking 17.9 mA. Moreover, a capacitor model for M-DEG is established, which well reveals the influence of the properties of dielectric layers and droplets on the electric output, and accurately predicts the results.

Keywords: energy harvest, droplet-based electricity generator, water energy, liquid-solid interface, electrical double layer

Introduction

The development of technology has leads to the increasingly severe energy crisis that has seriously affected normal production and living standards[1-3]. One of most promising strategies to address this crisis is to harvest energy from clean and renewable water energy[4], which has inspired several new energy harvesting technologies[5-12], such as reverse electrowetting[13], liquid-solid-based triboelectric nanogenerators[14-17], hydrovoltaic technology[18, 19], and other related techniques[20-23]. Although diverse water-based electricity generators can harvest energy from various forms of water, the common fundamental mechanism lies in the dynamic interfacial liquid-solid interaction[24], which leads to the limited energy power density and energy conversion efficiency[15] in spite of a variety of optimization methods[16, 25-31].

Recently, a droplet-based electricity generator (DEG) with a transistor-inspired structure consisting of two electrodes and a single dielectric layer has been reported[32], where the transistor-like structure converts the interface effect into the bulk effect and greatly improves the energy conversion efficiency, which has triggered a research wave on the DEGs[33-36]. Besides, it has been shown that various treatment methods can improve the output performance of DEGs, including localized charge injection[37, 38], hydrophobic treating surface[39], interfacial laser-induced hydrophobic electrode[40], and dielectric layer/droplet optimization[41]. Furthermore, the falling height and hitting position of the droplet, and installation angle also influence the electric output of the DEGs[42].

Although several works have been made to improve the performance of DEG[43, 44], its

integration and application scalability are not well addressed. This is because the fact that DEG requires a hydrophobic surface with a high electron affinity such as polytetrafluoroethylene (PTFE) and fluorinated ethylene propylene (FEP) to achieve high surface density charge, which place a difficulty in the combination between the DEG and the daily materials. In this work, we propose a multiple dielectric layers-based DEG (M-DEG) featuring a middle layer that can be made of host material of daily goods. The introduction of a middle layer not only endows the DEG with the additional function, but greatly enhance its electrical performance. We demonstrate the electrical output of M-DEG could be mediated by the surface charge and relative permittivity of the dielectric layer 2, and the property of the droplet. The results is in good agreement with our capacitor model. Based on this, the M-DEG shows high flexibility and can be combined with daily objects (e.g. household glass and umbrellas), exhibiting the outstanding ability to harvest energy from precipitation.

Results

Our proposed M-DEG consists of a PTFE layer (dielectric layer 1), a polyimide film (PI, dielectric layer 2), a top steel electrode, and a bottom ITO electrode under the polyimide film (Figure 1a). We chose the PTFE film owing to the following reasons. The PTFE film is smooth and hydrophobic with a low surface roughness of 50.7 nm and a contact angle of 102.8° (Figure S1a, b), which achieves the efficient contact and separation of water droplets from the surface. In addition, the PTFE has high surface charge density owing to its electron-accepting fluorine group, whose presence can be evidenced by X-ray photoelectron spectroscopy (XPS) showing the obvious F 1s peak observed at 687 eV (Figure S1c).

To confirm the superiority of the dielectric layer 2, we first measured the open circuit voltage (V_{oc}) of the M-DEG containing a 30 μm PTFE layer (dielectric layer 1) and a 70 μm thick polyimide layer (dielectric layer 2). The result shows that the M-DEG generated a typical V_{oc} of 192.0 V, which increased by 26.3% compared to the ordinary DEG containing a 100 μm thick PTFE layer (Figure 1b), indicating that the multilayer structure has certain advantages over a single dielectric layer in spite of the same total thickness of the dielectric layers. We then investigated the effects of the thickness of the dielectric layers 1 (d_1) and 2 (d_2) on the electrical output. When d_2 is 25 μm, the V_{oc} and I_{sc} increased from 92.9 to 169.0 V and from 33.5 μA to 44.0 μA with the increase of d_1 from 30 to 100 μm, respectively (Figure S2a). In addition, when the dielectric layer 1 was 30 μm, the introduction of a 25 μm thick dielectric layer 2 could make V_{oc} and I_{sc} increase to 125.3 V (increased by 22.6%) and 33.2 μA (increased by 39.5%), as shown in Figure 1c. Then, V_{oc} and I_{sc} further increased to 194.8 V and 40.15 μA with the increase of d_2 to 100 μm, which was about 90.6% and 68.7% higher than that without the dielectric layer 2, respectively. Furthermore, it was found that the surface charge density of the upper surface of the dielectric layer 2 (σ_{21}) influenced the electrical output greatly. When the upper surface of the dielectric layer 2 was negatively charged ($\sigma_{21}<0$), the maximum V_{oc} was 150.0 V (Figure 1d). When σ_{21} was higher than 0, the V_{oc} was the lowest, only about 53.7 V. When σ_{21} was equal to 0, the V_{oc} was 133.3 V. These results showed that the property of the surface charge on the upper surface of the dielectric layer 2 significantly affected the V_{oc}.

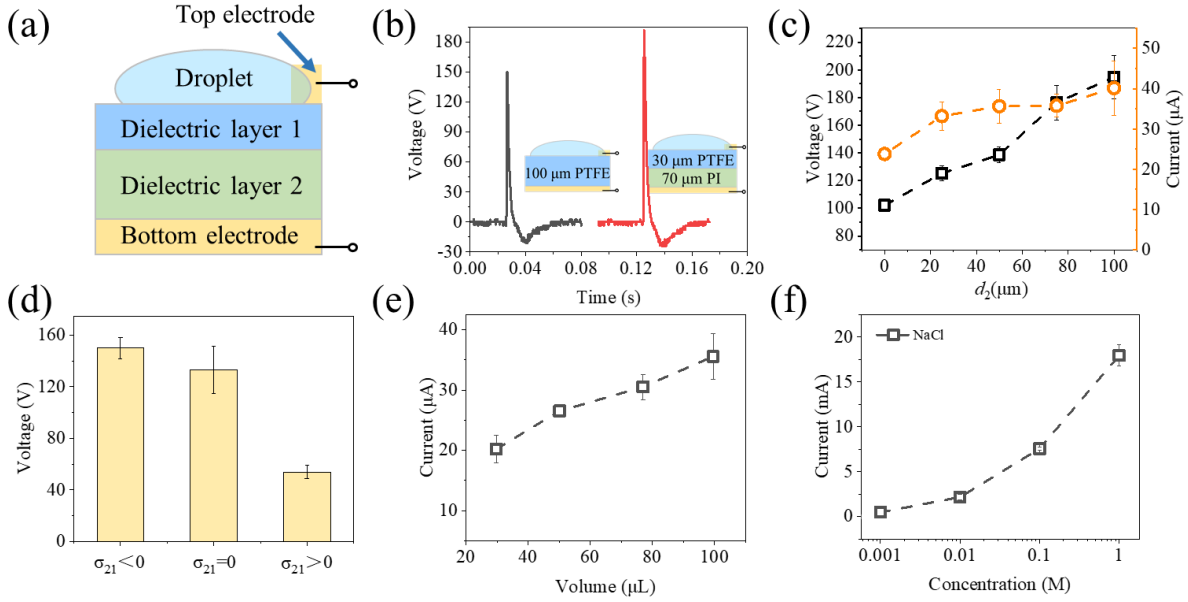

Figure 1. Electrical output of the M-DEG. (a) Structure of the M-DEG. (b) Typical voltage signals generated by the original DEG without the dielectric layer 2 and the M-DEG with the dielectric layer 2, respectively. The dielectric layer's total thickness of DEG is equal to that of the M-DEG. (c) Dependence of the V_{oc} and I_{sc} on the thickness of the dielectric layer 2 (d_2). The error bars are the SD values of 5 samples. (d) Relationship between the surface charge of the dielectric layer 2's upper surface (σ_{21}) and the V_{oc}. The error bars are the SD values of 3 samples. (e) Relationship between the I_{sc} and the volume of the droplet. The error bars are the SD values of 7 samples. (f) Dependence of the I_{sc} on the concentration of the NaCl. The error bars are the SD values of 7 samples. To our knowledge, this current value is much higher than the previously reported values generated by water-solid electricity generators[14, 32, 38, 41, 45-47].

We then investigated the effect of the property of the droplet on the I_{sc}. With the droplet volume increasing from 29.8 μL to 99.5 μL, the I_{sc} increases from 20.2 μA to 35.6 μA (Figure

1e). Further, the I_{sc} increases from 22.5 μA to 17.9 mA with the concentration of NaCl solution increasing from 10^{-7} M (DI water) to 1 M (Figure 1f). To our knowledge, this current value is much higher than the previously reported values generated by water-solid electricity generators (Figure S2b and Table S1).[14, 32, 38, 41, 45-47] Considering that the increase in NaCl concentration leads to the increase in droplet conductivity, the resistance of droplet may have a great influence on the I_{sc}.

Discussion

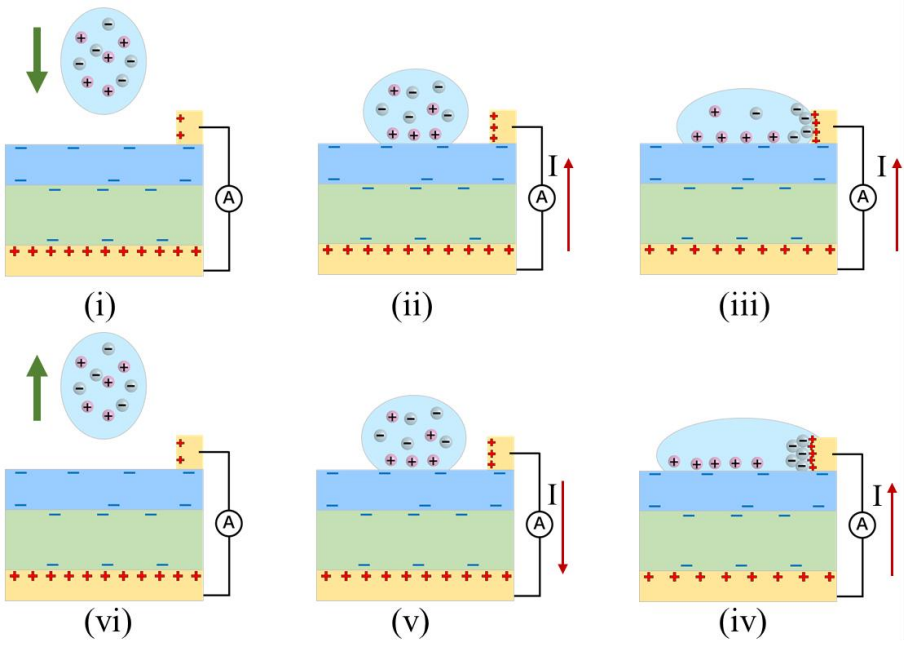

Figure 2. Mechanism of electricity generation. Figure (i)-(vi) show the charge carrier behavior when the droplet is in different positions. The surface charges of dielectric layer 1 or 2 are set as negative, which can be achieve by ion injection.

The transfer of charge between the droplets and the dielectric layer 1 is the basis for the electricity generation of M-DEG. We compared the amount of charge carried by the droplets

in two different cases (the schematic diagram of the experimental setup can be seen in Figure S3a, b): (i) the droplet falling directly into the Faraday cup directly, and (ii) the droplet falling into the Faraday cup after contacting the dielectric layer 1. The results showed that the total charge carried by 50 droplets without contacting the dielectric layer 1 was 0.02 nC, while that of 50 droplets after contacting the dielectric layer 1 was 38.49 nC (Figure S3c). After contacting the dielectric layer 1, the droplets carried much more charges, indicating that efficient charge transfer occurred between the droplets and the dielectric layer 1. The charge transfer between water and dielectric layer can be attributed to the mixed mechanism caused by the electron transfer and ion transfer, and the electron transfer dominates, which can be explain by the electron cloud model (Figure S3d)[48-50]. The electricity generation mechanism of the M-DEG is illustrated by a typical current period in Figure S4 combined with the schematic diagram in Figure 2. Before the droplet contacts the surface of the dielectric layer 1, the charge of each part of the M-DEG is balanced. In this case, there is no current, corresponding to Figure 2(i). When the droplet contacts the upper surface of the dielectric layer 1 and the top electrode and then spreads, the charges inside the droplet move directionally to form electrical double layers (EDLs) at the liquid-dielectric layer 1 interface and the liquid-top electrode interface (Figure 2(ii)-(iv)). In this process, the initial local charge balance is broken, and a current is generated to restore the charge balance. When the contact area between the droplet and surface decreases, the EDLs disappear, corresponding to a reverse current (Figure 2(v)). When the droplet is completely detached from the dielectric layer 1, the charge balance is re-established and the current disappears (Figure 2(vi)).

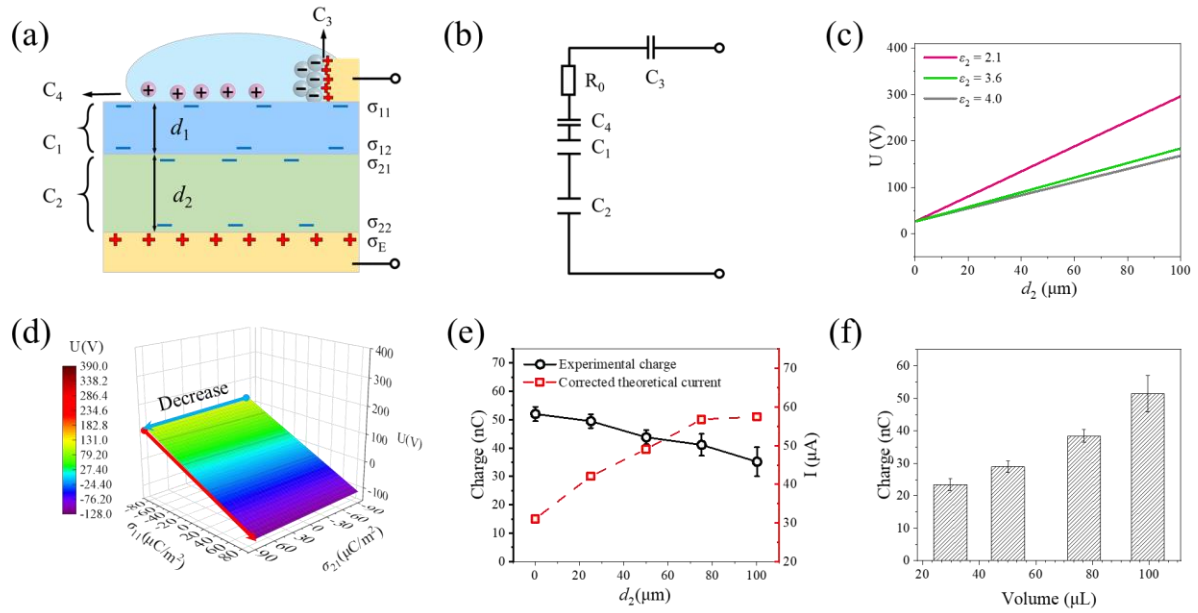

Figure 3. Theoretical potential difference and current of the M-DEG. (a) Schematic of the M-DEG. The surface charges of dielectric layer 1 or 2 are negatively charged by ion injection. (b) Equivalent circuit of (a). (c) Dependence of the theoretical potential difference on the d_2. The smaller relative permittivity of the dielectric layer 2 results in a faster increasing rate of the potential difference. (d) Theoretical potential difference modulated by both the surface charge density of upper surface of the dielectric layers 1 (σ_{11}) and 2 (σ_{21}). By regulating σ_{11} and σ_{21}, the potential difference can be changed from positive to negative. (e) Dependence of the corrected theoretical current and experimental transferred charge on d_2. The error bars are the SD values of 3 samples. (f) Relationship between the transfer charge and the volume of the droplet. The PTFE is used as the dielectric layer 1, and PI is used as the dielectric layer 2. The error bars are the SD values of 7 samples. The relative permittivity and surface charge densities of the dielectric layers were taken from the literature values[51-56].

To understand the mechanism of the M-DEG, we build an equivalent circuit model and explore the effect of various factors on the electrical output. When the droplet contacts the M-

DEG, the anions and cations in the droplet migrate to the surfaces of the top electrode and the dielectric layer 1, respectively (Figure 3a). The EDL will form at the droplet-dielectric layer 1 interface and the droplet-top electrode interface. Thus, the capacitor model for the M-DEG is proposed, which can be further simplified in Figure 3b. The dielectric layers 1 and 2 are regarded as two capacitors C_1 and C_2, respectively. The EDL capacitors forms at the droplet-top electrode interface and the droplet-dielectric layer 1 interface are C_3 and C_4, respectively. The internal resistance of M-DEG is R_0. The theoretical potential difference between the top and bottom electrodes is given by Equation 1 (see Figure S5 and Note S1 in the supporting information for the detailed derivation),

$$U = \frac{(\sigma_{12} + \sigma_{21} - \sigma_{11})d_1}{2\varepsilon_1\varepsilon_0} + \frac{(\sigma_E + \sigma_{22} - \sigma_{12} - \sigma_{21})d_2}{2\varepsilon_2\varepsilon_0} \quad (1)$$

where σ_{11}, σ_{12}, σ_{21}, and σ_{22} are the upper and lower surface charge densities of the dielectric layers 1 and 2, respectively. σ_E is the induced charge density of the bottom electrode. d_1 and d_2 are the thickness of the dielectric layers 1 and 2, respectively. One thing to note is that the surface charge density is not an absolute value in our work. ε_0 is the vacuum dielectric permittivity. ε_1 and ε_2 are the relative permittivity of the dielectric layers 1 and 2, respectively. Since σ_E is generated by electrostatic induction and the thickness of two dielectric layers is small, regardless of the environmental impact, there should be the following relationship: $\sigma_{11} + \sigma_{12} + \sigma_{21} + \sigma_{22} + \sigma_E = 0$. Equation 1 can be simplified as,

$$U = -\frac{(2\sigma_{12} + 2\sigma_{21} + \sigma_{11})d_2}{2\varepsilon_2\varepsilon_0} + \frac{(\sigma_{12} + \sigma_{21} - \sigma_{11})d_1}{2\varepsilon_1\varepsilon_0} \quad (2)$$

Equation 2 shows that the theoretical potential difference of M-DEG is related to the thickness,

relative permittivity, and surface charge densities of the dielectric layers 1 and 2.

According to Equation 2, the theoretical potential difference between the top and bottom electrodes of the M-DEG is directly affected by d_1. When d_1 increases from 0 to 50 μm, the theoretical potential difference increases linearly from 0 to 321.5 V (Figure S6a). Since the theoretical potential difference between the top and bottom electrodes of the M-DEG is the driven force of the electrical output, the V_{oc} also increases with the d_1 (Figure S2a). However, further experiment showed that the V_{oc} increased from 169.0 V to 196.9V with the increase of d_1 from 100 to 300 μm. And then it started to decrease when d_1 was larger than 300 μm (Figure S6b). Considering that the generation of electricity involves charge exchange and the flow of charge induced by electrostatic induction, a too large d_1 may affect the electrostatic induction, leading to the decrease of the electrical output. The effect of the d_2 on the theoretical potential difference shows that the theoretical potential difference increases from 26.2 to 179.3 V with d_2 increasing from 0 μm to 100 μm, as shown in Figure 3c. This provides a reasonable explanation for the V_{oc} increasing with the increase of the d_2 (Figure 1c). Further, it is found that the higher relative permittivity of the dielectric layer 2 is not conducive to the increase of voltage. The σ_{11} and σ_{21} also influence the theoretical potential difference (Figure 3d). The theoretical potential difference decreases with the increase of σ_{21}, which is consistent with the experiment results (Figure 1d). Further, the theoretical potential difference decreases sharply from 107.2 V to -114.3 V with σ_{11} increasing from -90 μC m^{-2} to 90 μC m^{-2} (σ_{21} remains at 90 μC m^{-2}). This result indicates that the surface charge on the upper surface of the dielectric layer

1 dominates the voltage output. Besides, the theoretical potential difference decreases with the increase of surface charge density on the σ_{12} (Figure S7). However, the σ_{22} has little effect on V_{oc} according to Equation 2.

In order to apply the M-DEG in practical application, the equivalent circuit model of the M-DEG should be further simplified as a series circuit, including a load resistance R_L, an internal resistance R_0, and an equivalent capacitance (C_E). The C_E is the equivalent capacitance for C_1, C_2 and C_4 (Figure S8a, b). The theoretical current (I) is given by Equation 3 (see Figure S8 and Note S2 in the supporting information for the detailed derivation),

$$I = \frac{Q}{\tau} = \frac{Q}{RC_E} = \frac{(\varepsilon_1 d_2 + \varepsilon_2 d_1)Q}{\varepsilon_1 \varepsilon_2 \varepsilon_0 AR} = \frac{(\varepsilon_1 d_2 + \varepsilon_2 d_1)}{\varepsilon_1 \varepsilon_2} \frac{Q}{\varepsilon_0 AR} \quad (3)$$

where Q is the total transferred charge, τ is the time constant, A is the spreading area of the droplet, and R is the total resistance ($R=R_0+R_L$). According to Equation 3, the theoretical current is affected by the amount of transferred charge, the thickness and relative permittivity of the dielectric layers 1 and 2, the spreading area of the droplet, and the resistance. The theoretical current increases from 17.2 μA to 45.1 μA with the increase of the d_1 from 30 μm to 100 μm (Figure S9a). However, the experimental I_{sc} slightly increases from 33.5 μA to 44.0 μA with the increase of d_1 from 30 μm to 100 μm (Figure S2a), indicating that the increase in experimental I_{sc} is smaller than the theoretical prediction. This is because the transferred charge decreases with the increase in thickness (Figure S9b). Since the transferred charge is the integral of the current over time, a slower increase in current with d_1 was observed experimentally. In addition, the increase in the d_2 can also enhance the theoretical current.

However, it should be noted that as the d_2 increased, the transferred charge gradually decreased (Figure 3e). Considering the coupling effect of the d_2 and the transferred charge on the theoretical current, the theoretical current has been corrected by substituting the experimental value of the transferred charge into Equation 3. The result shows that when d_2 increases from 0 to 100 μm, the corrected theoretical current increases from 31.1 μA to 57.5 μA (Figure 3e), which well explains the experimental results in Figure 1c. At the same time, it also enlightened us that the amount of transferred charge is crucial to the experimental I_{sc}. We, therefore, investigated the relationship between the amount of transferred charge and the droplet volume. The result showed that the transferred charge increased from 23.5 nC to 51.4 nC with the increase of droplet volume from 29.8 μL to 99.5 μL (Figure 3f). This was a good explanation for the increase of the experimental I_{sc} with the increase of the droplet volume (Figure 1e).

The optimization of output current also demands a delicate control of circuit resistance (Figure S10a). When the circuit resistance is in the range of 5×10^6~1.5×10^7 Ω, corresponding to the resistance of the DI water droplet, the theoretical current is tens of μA. When the circuit resistance decreases, the theoretical current will increase rapidly. It would increase to greater than 1 mA when the circuit resistance decreases to less than 3.3×10^5 Ω. In our experiments, when the NaCl solution droplet (concentration: 1 M, resistance: 105.9 ~ 119.3 kΩ) was used (Figure S10b-e), the experimental I_{sc} was 17.9 mA (Figure 1f), which was in good agreement with the theoretical calculation. Moreover, compared with the deionized water, the ions in NaCl can generate the stronger periodic shielding of surface charges, which is conducive to larger currents. In addition, we compared the transferred charges of the original DEG and the M-DEG

by using a 1 M NaCl solution. The results showed that the introduction of the dielectric layer 2 led to more transferred charges of the M-DEG, which may be related to the charge on the surface of the dielectric layer 2 (Figure S11a). It is also found that the introduction of the dielectric layer 2 will results in a larger equivalent capacitance (see Figure S11b-c and Note S3 in the supporting information for the detailed derivation), which is also beneficial for more transfer charges, leading to the higher current.

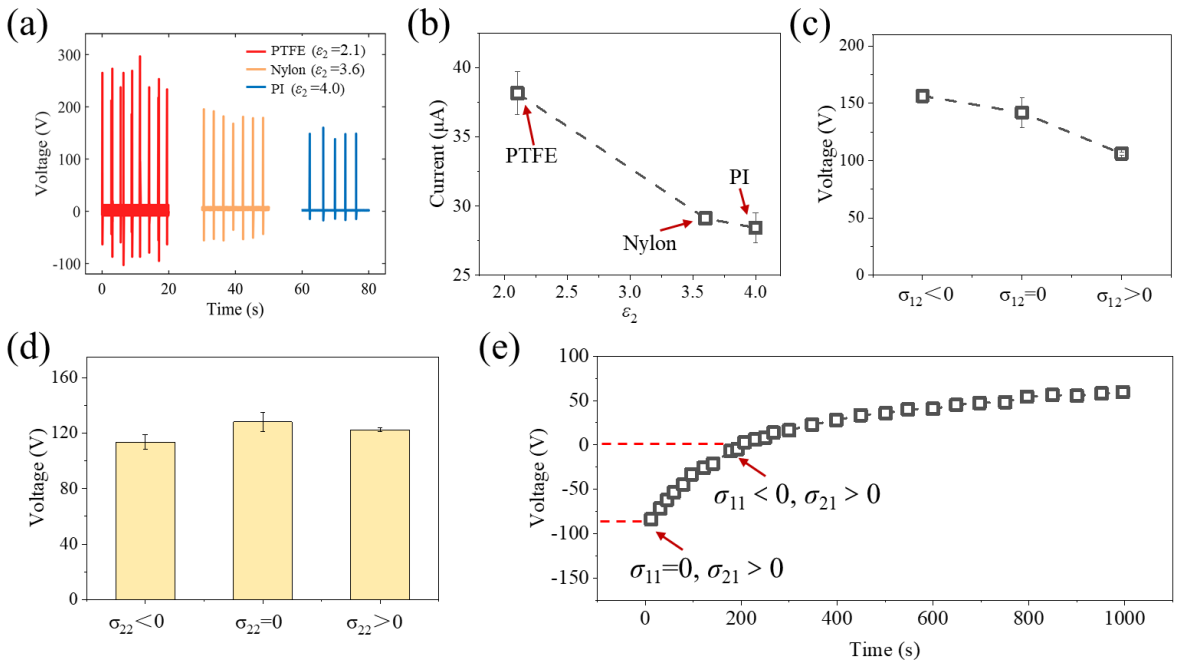

Figure 4. Validation of capacitor models. (a) V_{oc} generated by using three different materials (PTFE, Nylon, and PI) as the dielectric layer 2. (b) Dependency of I_{sc} on the ε_2. (c) Relationship between the σ_{12} and V_{oc}. (d) Relationship between the σ_{22} and V_{oc}. The error bars in (b-d) are the SD values of 3 samples. (e) Evolution of V_{oc} with droplet impact.

According to Equation 2 and Equation 3, the V_{oc} and I_{sc} are both negatively correlated with ε_2, indicating that they are closely related to the material of the dielectric layer 2. The PTFE (ε_2

= 2.1), Nylon (ε_2 = 3.6), and PI (ε_2 = 4.0) were chosen as the dielectric layer 2 for comparison, respectively. The results of V_{oc} showed that using the PTFE, Nylon, and PI film had the V_{oc} of 278.0 V, 187.0 V, and 151.7 V, respectively (Figure 4a). The results of I_{sc} showed that I_{sc} reached a maximum value of 38.2 μA when the PTFE was used as the dielectric layer 2 (Figure 4b). PI film produced the lowest I_{sc} of 28.4 μA. The V_{oc} and I_{sc} decrease with the increase of the relative permittivity of the dielectric layer 2. Furthermore, according to Equation 2, V_{oc} decreases with the increase of the σ_{12}, which is confirmed by the experimental results (Figure 4c). When the lower surface of the dielectric layer 1 was negatively charged ($\sigma_{12}<0$), the maximum V_{oc} was 156.4 V. The positively charged lower surface of dielectric layer 1 ($\sigma_{12}>0$) generated the lowest V_{oc} of 106.1 V. When σ_{12} was equal to 0, the V_{oc} was 141.8 V. Unlike other surfaces, the σ_{22} does not affect the potential difference according to Equation 2, indicating that σ_{22} does not affect the V_{oc} (Figure 4d). Moreover, the reversal of the potential difference is more likely to occur by regulating both σ_{11} and σ_{21} according to Equation 2. We first removed the charges on the surfaces of the dielectric layers 1 (PTFE) and 2 (PI) and then used the antistatic gun to positively charge the upper surface of the dielectric layer 2. Under the impinging of the first droplet, the M-DEG produced a negative V_{oc} of -83.9 V (Figure 4e). As the droplet continued to hit the surface of the dielectric layer 1, the charge transfer occurred between the droplet and the dielectric layer 1. Thus, the upper surface of the dielectric layer 1 gradually became negatively charged, and the V_{oc} became 0 V when the negative charges on the upper surface of the dielectric layer 1 and the positive charges on the upper surface of the dielectric layer 2 contributed equally. As the negative charge of the dielectric layer 1 continued

to increase, the V_{oc} reversed to positive and then continued to increase over time until it stabilized. The above experimental results are accurately predicted by Equation 2 and Equation 3, further validating our capacitor model. All of the analysis indicates that the introduction of the dielectric layer 2 could enhance the equivalent capacitance of the entire system and endow more surface charge involving in the electricity generation. The equation 2 and 3 derived by the capacitor model can also guide us the chosen of the parameters to achieve higher electric output. In addition, our capacitor model can further explain the electrical output of more complex DEG, such as the M-DEG with three dielectric layers (see Note S4 and Figure S12 in the supporting information for detailed information).

Benefiting from the introduction of the dielectric layer 2, M-DEG can be combined with various daily objects to harvest the energy of droplets. To explore the application potential of the M-DEG, we next tested the electric output of M-DEG with glass as the dielectric layer 2. The results showed the V_{oc} reached a maximum value of 268.0 V when the glass thickness was 0.55 mm (Figure S13a). When the glass thickness reached 4 ~ 6 mm (the thickness of common household glass), the V_{oc} of M-DEG was still as high as 106.4 ~ 121.2 V (powering 50 LEDs), which provided a potential for the design of smart household windows to harvest energy (Figure S13b). Thereafter, a piece of 200 mm × 200 mm × 4 mm household window was combined with an FEP film to prepare a window-based energy source (WES), as shown in Figure 5a. There were 9 pieces of 50 mm × 50 mm rectangular ITO layer at the bottom of WES as the bottom electrodes, and 3 extremely thin wires at the top as the top electrodes. Three M-

DEGs in a row acted as an energy unit. Thanks to the transparent ITO and FEP, WES had good transparency (Figure S13c-d). We tested the electrical output of the WES by using 0.001 M NaCl. The results showed that an energy unit of WES generated a maximal V_{oc} of 160.0 V and an I_{sc} of 792.0 μA (Figure S13e) and two energy units could power two "SKLT" LED patterns with 85 LEDs (Figure S13d and Video S1). In addition, the output energy of the WES could also be stored in capacitors. Two energy units of the WES were connected with commercial capacitors and the voltage-time curves were measured. The result showed that the commercial capacitors of 1 μF, 3 μF, and 10 μF could be charged to 12.6 V, 7.0 V, and 3.0 V at 5.1 Hz after 295 ± 2.5 s, respectively (Figure 5b). The charge amount charged by a single droplet was 5.3 times higher than that in the previous work[39]. Furthermore, an umbrella made of polyester fiber was used as the dielectric layer 2 to fabricate an umbrella-based energy source (UES). The dielectric layer 1 was made of PTFE film, and the bottom and top electrodes are both made of copper tapes (Figure 5c). UES could not only block the wind and rain but also could power the LEDs on rainy nights. Eight LEDs were installed on the eight tips of the UES and an "SKLT" LED pattern was connected to nine energy units by wires. When a handheld shower was used to simulate rain, UES could power an "SKLT" LED pattern and the LEDs on the tips of the UES, which could be used for position warnings in the dark (Figure 5d and Video S2). A good combination of M-DEG with goods such as umbrellas and windows demonstrates its strong application potential for energy harvest in daily life.

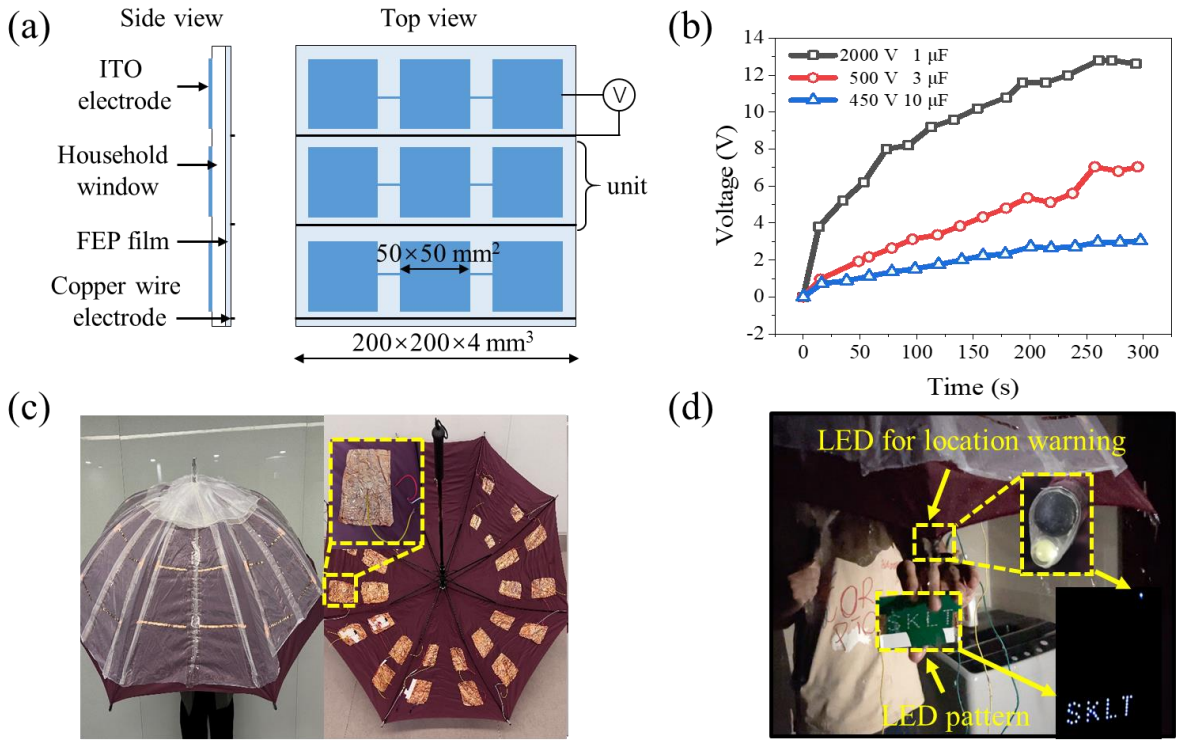

Figure 5. Application of the M-DEG. (a) Schematic diagram of window-based energy source (WES). Three M-DEGs in a row act as an energy unit. (b) Charging curves of commercial capacitors of 1 μF, 3 μF, and 10 μF using two energy units of WES (droplet impinging frequency: 5.1 Hz). (c) Structure of the umbrella-based energy source (UES). (d) Photo of the UES, including position warning and powering the LED pattern.

Conclusion

In our work, a sandwich-structured multiple dielectric layers-based DEG (M-DEG) consisting of the top and bottom electrodes, and two dielectric layers has been fabricated. The introduction of a dielectric layer 2 enhanced the V_{oc} and I_{sc} by 90.6% and 68.7%, which reached 194.8 V and 40.15 μA, respectively. The equivalent capacitor model for M-DEG has been built, which essentially reveals how the properties of the droplet and dielectric layers affect the

electrical output of the M-DEG. The increase of the dielectric layers' thickness and solvent concentration of the droplet can greatly increase the voltage and current, respectively. Interestingly, the effect of the surface charge on the dielectric layers except that on the lower surface of the dielectric layer 2 on the voltage is quite obvious. In addition, the M-DEG can be combined with daily objects such as umbrellas and windows due to the electrical output of M-DEG being not sensitive to thickness, which could make them harvest energy from the rainwater without interfering with their original function. This work provides profound guidance for the optimization of droplet-based electricity generators and greatly develops the application potential of DEG.

Experiment section

Materials and Preparation of the M-DEG.

All materials are obtained from suppliers without any preprocessing. The M-DEG consisted of a PTFE film (30 mm long, 30 mm wide) as the dielectric layer 1 and a dielectric layer 2 (30 mm long, 30 mm wide, using PI, PVC, and Nylon). The ITO glass and a 304 stainless steel needle were used as the bottom electrode and the top electrode, respectively. The relative permittivity of PTFE, PI, and Nylon are 2.1, 3.6, and 4.0, respectively. Specific steps are as follows: (1) Cut the required material to the correct size; (2) Ionizing air blowers (Ionizing air blowers, BaKon BK5600, Shenzhen BaKon Electronic Technology Co., LTD, China) was used to remove initial surface charge of the materials; (3) Positive charge (negative charge) was injected onto the upper surface of the dielectric layer 2 by using antistatic gun (Zerostat3, Milty),

corresponding to $\sigma_{21} > 0$ ($\sigma_{21} < 0$). If the antistatic gun was not used, σ_{21} should be considered approximately equal to 0. (4) Fabrication.

Measurement of the electric output.

The liquid is driven through the pipe by the syringe and drips from the outlet of the pipe with a height of 50 cm. At the moment the falling droplet hit the upper surface and the top electrode of the M-DEG, electricity is generated. The height of the M-DEG is 15 cm. The voltage output of the M-DEG was measured by an oscilloscope (RTE1024, Rohde and Schwarzrte, Germany) equipped with a high-impedance (10 MΩ) probe. The current was measured using the oscilloscope coupled with a low-noise current preamplifier (Model SR570, Stanford Research System, USA). The charge was measured by using the oscilloscope coupled with a nanocoulomb meter (MONROE 284, Monroe Electronics Inc., USA). All tests are performed at room temperature.

Measurement of charge carried by the droplet.

The charge carried by the droplet was measured by the Faraday cup (JBNFLD-20203001, Beijing Jinbeinuo Technology Co., Ltd., China) and nanocoulomb meter (MONROE 284, Monroe Electronics Inc., USA). The liquid is driven through the pipe by the syringe and drips from the outlet of the pipe. There is a wire at the outlet of the pipe connected to the ground, which can neutralize the electric charge of the droplet rubbing against the pipe. Subsequently, the droplet falls directly into the Faraday cup, and the nanocoulomb meter will record the charge carried by the droplet without contacting the M-DEG. In another condition, the falling

droplet will contact the M-DEG first and then falls into the Faraday cup. The charge carried by the droplet contacting the M-DEG will be recorded by the nanocoulomb meter.

Characterization of the materials.

The surface morphology and roughness were observed by the atomic force microscope (AFM, MFP-3D, Oxford Instruments, UK). The chemical elements of the materials were characterized by XPS (PHI Quantera II, Ulvac-Phi, Japan). Static contact angles of water on the PTFE were measured by using a Dataphysics OCA25 video-based optical angle measuring system at room temperature.

Calculation of the potential difference, current, and simulation of potential distribution.

During the calculation of the potential difference and the current, the surface charge density and relative permittivity of the dielectric layer were quoted from literature values[51-58]. The relative permittivity of PTFE, PI, and Nylon are 2.1, 3.6, and 4.0, respectively. The surface charge density of the upper surface and lower surface of the dielectric layer 1 (PTFE) are -50 $\mu C\ m^{-2}$ and – 20 $\mu C\ m^{-2}$, respectively. The surface charge density of the dielectric layer 2 (PI) is -15.47 $\mu C\ m^{-2}$. Unless otherwise specified, the thickness of the dielectric layer 1 and dielectric layer 2 is 30 μm and 100 μm, respectively.

Credit authorship contribution statement

Kaiqiang Wang: Conceptualization, Writing-Original Draft, Methodology, Investigation, Data Curation, Visualization, Formal analysis, Software, Writing - Review & Editing. **Wanghuai Xu:** Conceptualization, Methodology, Investigation, Data Curation, Formal analysis, Writing - Review & Editing. **Jianfeng Li:** Methodology, Investigation, Visualization. **Huanxi Zheng:** Methodology, Investigation. **Shouyi Sun:** Methodology, Investigation, Visualization. **Wei Song:** Methodology, Investigation, Visualization. **Yuxin Song:** Methodology, Investigation. **Zhengmao Ding:** Visualization. **Rui Zhang:** Methodology. **Yilin Sun:** Investigation. **Hanli Zhang:** Investigation. **Jinjin Li:** Writing - Review & Editing, Methodology, Conceptualization, Formal analysis, Supervision, Project administration, Funding acquisition. **Zuankai Wang:** Writing - Review & Editing, Methodology, Conceptualization, Formal analysis, Supervision, Project administration.

Acknowledgements

We acknowledge the financial support from National Key R&D Program of China (2020YFA0711003), the National Natural Science Foundation of China (No. 51775295 and No. 52175174), and the Open Research Fund of Jiangsu Key Laboratory for Design and Manufacture of Micro-Nano Biomedical Instruments (No. KF202004).

Declaration of Competing Interest

The authors declare that they have no known competing financial interests or personal relationships that could have appeared to influence the work reported in this paper.

Reference

[1] W. Xu, Z. Wang, Fusion of Slippery Interfaces and Transistor-Inspired Architecture for Water Kinetic Energy Harvesting, Joule, 4 (2020) 2527-2531.

[2] K. Wang, J. Li, J. Li, C. Wu, S. Yi, Y. Liu, J. Luo, Hexadecane-containing sandwich structure based triboelectric nanogenerator with remarkable performance enhancement, Nano Energy, 87 (2021) 106198.

[3] K. Wang, C. Wu, H. Zhang, J. Li, J. Li, Cylindrical bearing inspired oil enhanced rolling friction based nanogenerator, Nano Energy, 99 (2022) 107372.

[4] Y. Yang, C. Lee, Making use of water droplets as a sustainable green energy source, Droplet, 1 (2022) 7-10.

[5] N. Zhang, H. Gu, H. Zheng, S. Ye, L. Kang, C. Huang, K. Lu, W. Xu, Q. Miao, Z. Wang, J. Zhang, X. Zhou, Boosting the output performance of volume effect electricity generator (VEEG) with water column, Nano Energy, 73 (2020) 104748.

[6] J. Yu, T. Ma, Triboelectricity-based self-charging droplet capacitor for harvesting low-level ambient energy, Nano Energy, 74 (2020) 104795.

[7] M. Chen, J. Chen, W. Zhou, X. Han, Y. Yao, C.-P. Wong, Realizing an All-Round Hydrogel Electrolyte toward Environmentally Adaptive Dendrite-Free Aqueous Zn–MnO2 Batteries, Advanced Materials, 33 (2021) 2007559.

[8] P. Hundekar, S. Basu, X. Fan, L. Li, A. Yoshimura, T. Gupta, V. Sarbada, A. Lakhnot, R. Jain, S. Narayanan, Y. Shi, C. Wang, N. Koratkar, In situ healing of dendrites in a potassium metal battery, Proceedings of the National Academy of Sciences, 117 (2020) 5588-5594.

[9] J. Han, S.G. Yoon, W.H. Lee, H. Jin, Y.H. Cho, Y.S. Kim, Ionic Diffusion-Driven Ionovoltaic Transducer for Probing Ion-Molecular Interactions at Solid–Liquid Interface, Advanced Science, 9 (2022) 2103038.

[10] H. Zhou, J. Dong, H. Liu, L. Zhu, C. Xu, X. He, S. Zhang, Q. Song, The coordination of displacement and conduction currents to boost the instantaneous power output of a water-tube triboelectric nanogenerator, Nano Energy, 95 (2022) 107050.

[11] J. Dong, C. Xu, L. Zhu, X. Zhao, H. Zhou, H. Liu, G. Xu, G. Wang, G. Zhou, Q. Zeng, Q. Song, A high voltage direct current droplet-based electricity generator inspired by thunderbolts, Nano Energy, 90 (2021) 106567.

[12] J. Dong, L. Zhu, P. Guo, C. Xu, X. Zhao, S. Yang, X. He, G. Zhou, G. Ma, H. Guo, C. Hu, Q. Song, A bio-inspired total current nanogenerator, Energy & Environmental Science, (2023).

[13] T. Krupenkin, J.A. Taylor, Reverse electrowetting as a new approach to high-power energy harvesting, Nature Communications, 2 (2011) 448.

[14] Z.-H. Lin, G. Cheng, S. Lee, K.C. Pradel, Z.L. Wang, Harvesting Water Drop Energy by a Sequential Contact-Electrification and Electrostatic-Induction Process, Advanced Materials, 26 (2014) 4690-4696.

[15] K. Wang, J. Li, Electricity generation from the interaction of liquid–solid interface: a review, Journal of Materials Chemistry A, 9 (2021) 8870-8895.

[16] H. Zhang, K. Wang, J. Li, J. Li, R. Zhang, Y. Zheng, Liquid-based nanogenerator fabricated by a self-assembled fluoroalkyl monolayer with high charge density for energy

harvesting, Matter, 5 (2022) 1466-1480.
[17] K. Wang, Y. Liu, J. Li, J. Li, Electricity generation by sliding an ionic solution droplet on a self-assembled reduced graphene oxide film, Journal of Materials Chemistry A, 8 (2020) 12735-12743.
[18] J. Yin, J. Zhou, S. Fang, W. Guo, Hydrovoltaic Energy on the Way, Joule, 4 (2020) 1852-1855.
[19] J. Yin, X. Li, J. Yu, Z. Zhang, J. Zhou, W. Guo, Generating electricity by moving a droplet of ionic liquid along graphene, Nature Nanotechnology, 9 (2014) 378-383.
[20] F. Zhao, Y. Liang, H. Cheng, L. Jiang, L. Qu, Highly efficient moisture-enabled electricity generation from graphene oxide frameworks, Energy & Environmental Science, 9 (2016) 912-916.
[21] B. Fan, A. Bhattacharya, P.R. Bandaru, Enhanced voltage generation through electrolyte flow on liquid-filled surfaces, Nature Communications, 9 (2018) 4050.
[22] X. Liu, H. Gao, J.E. Ward, X. Liu, B. Yin, T. Fu, J. Chen, D.R. Lovley, J. Yao, Power generation from ambient humidity using protein nanowires, Nature, 578 (2020) 550-554.
[23] L.E. Helseth, Harvesting energy from light and water droplets by covering photovoltaic cells with transparent polymers, Applied Energy, 300 (2021) 117394.
[24] W. Kaiqiang, X. Wanghuai, Z. Wei, W. Xiong, Y. Xiao, L. Jianfeng, Z. Hanli, L. Jinjin, W. Zuankai, Bio-inspired water-driven electricity generators: From fundamental mechanisms to practical applications, Nano Research Energy, (2023).
[25] J. Fu, G. Xu, H. Wu, C. Li, Y. Zi, Liquid-Interfaces-Based Triboelectric Nanogenerator: An Emerging Power Generation Method from Liquid-Energy Nexus, Advanced Energy and Sustainability Research, n/a (2022) 2200051.
[26] J. Park, S. Song, Y. Yang, S.H. Kwon, E. Sim, Y.S. Kim, Identification of Droplet-Flow-Induced Electric Energy on Electrolyte-Insulator-Semiconductor Structure, J Am Chem Soc, 139 (2017) 10968-10971.
[27] J. Niu, W. Xu, K. Tian, G. He, Z. Huang, Q. Wang, Triboelectric Energy Harvesting of the Superhydrophobic Coating from Dropping Water, Polymers, 12 (2020) 1936.
[28] H. Wang, Y. Sun, T. He, Y. Huang, H. Cheng, C. Li, D. Xie, P. Yang, Y. Zhang, L. Qu, Bilayer of polyelectrolyte films for spontaneous power generation in air up to an integrated 1,000 V output, Nature Nanotechnology, 16 (2021) 811-819.
[29] Y. Jin, C. Wu, P. Sun, M. Wang, M. Cui, C. Zhang, Z. Wang, Electrification of water: From basics to applications, Droplet, 1 (2022) 92-109.
[30] X. Leng, L. Sun, Y. Long, Y. Lu, Bioinspired superwetting materials for water manipulation, Droplet, 1 (2022) 139-169.
[31] A. Laroche, A. Naga, C. Hinduja, A.A. Sharifi, A. Saal, H. Kim, N. Gao, S. Wooh, H.-J. Butt, R. Berger, D. Vollmer, Tuning static drop friction, Droplet, 2 (2023) e42.
[32] W. Xu, H. Zheng, Y. Liu, X. Zhou, C. Zhang, Y. Song, X. Deng, M. Leung, Z. Yang, R.X. Xu, Z.L. Wang, X.C. Zeng, Z. Wang, A droplet-based electricity generator with high instantaneous power density, Nature, 578 (2020) 392-396.
[33] L.E. Helseth, A water droplet-powered sensor based on charge transfer to a flow-through front surface electrode, Nano Energy, 73 (2020) 104809.

[34] N. Zhang, H. Gu, K. Lu, S. Ye, W. Xu, H. Zheng, Y. Song, C. Liu, J. Jiao, Z. Wang, X. Zhou, A universal single electrode droplet-based electricity generator (SE-DEG) for water kinetic energy harvesting, Nano Energy, 82 (2021) 105735.
[35] L. Wang, W. Li, Y. Song, W. Xu, Y. Jin, C. Zhang, Z. Wang, Monolithic Integrated Flexible Yet Robust Droplet-Based Electricity Generator, Advanced Functional Materials, 32 (2022) 2206705.
[36] H. Zheng, H. Wu, Z. Yi, Y. Song, W. Xu, X. Yan, X. Zhou, S. Wang, Z. Wang, Remote-Controlled Droplet Chains-Based Electricity Generators, Advanced Energy Materials, (2023) 2203825.
[37] H. Wu, R. Dey, I. Siretanu, D. van den Ende, L. Shui, G. Zhou, F. Mugele, Electrically Controlled Localized Charge Trapping at Amorphous Fluoropolymer–Electrolyte Interfaces, Small, 16 (2020) 1905726.
[38] H. Wu, N. Mendel, S. van der Ham, L. Shui, G. Zhou, F. Mugele, Charge Trapping-Based Electricity Generator (CTEG): An Ultrarobust and High Efficiency Nanogenerator for Energy Harvesting from Water Droplets, Adv Mater, 32 (2020) e2001699.
[39] L. Wang, Y. Song, W. Xu, W. Li, Y. Jin, S. Gao, S. Yang, C. Wu, S. Wang, Z. Wang, Harvesting energy from high-frequency impinging water droplets by a droplet-based electricity generator, Ecomat, 3 (2021) e12116.
[40] Y. Chen, B. Xie, J. Long, Y. Kuang, X. Chen, M. Hou, J. Gao, S. Zhou, B. Fan, Y. He, Y.-T. Zhang, C.-P. Wong, Z. Wang, N. Zhao, Interfacial Laser-Induced Graphene Enabling High-Performance Liquid−Solid Triboelectric Nanogenerator, Advanced Materials, 33 (2021) 2104290.
[41] N. Zhang, H. Zhang, W. Xu, H. Gu, S. Ye, H. Zheng, Y. Song, Z. Wang, X. Zhou, A droplet-based electricity generator with ultrahigh instantaneous output and short charging time, Droplet, 1 (2022) 56-64.
[42] X. Wang, S. Fang, J. Tan, T. Hu, W. Chu, J. Yin, J. Zhou, W. Guo, Dynamics for droplet-based electricity generators, Nano Energy, 80 (2021).
[43] S. Li, J. Nie, Y. Shi, X. Tao, F. Wang, J. Tian, S. Lin, X. Chen, Z.L. Wang, Contributions of Different Functional Groups to Contact Electrification of Polymers, Adv Mater, 32 (2020) 2001307.
[44] F. Zhan, A.C. Wang, L. Xu, S. Lin, J. Shao, X. Chen, Z.L. Wang, Electron Transfer as a Liquid Droplet Contacting a Polymer Surface, ACS Nano, 14 (2020) 17565-17573.
[45] L.E. Helseth, X.D. Guo, Contact Electrification and Energy Harvesting Using Periodically Contacted and Squeezed Water Droplets, Langmuir, 31 (2015) 3269-3276.
[46] B. Kil Yun, H. Soo Kim, Y. Joon Ko, G. Murillo, J. Hoon Jung, Interdigital electrode based triboelectric nanogenerator for effective energy harvesting from water, Nano Energy, 36 (2017) 233-240.
[47] L. Liu, Q. Shi, J.S. Ho, C. Lee, Study of thin film blue energy harvester based on triboelectric nanogenerator and seashore IoT applications, Nano Energy, 66 (2019) 104167.
[48] C. Xu, Y. Zi, A.C. Wang, H. Zou, Y. Dai, X. He, P. Wang, Y.-C. Wang, P. Feng, D. Li, Z.L. Wang, On the Electron-Transfer Mechanism in the Contact-Electrification Effect, Advanced Materials, 30 (2018) 1706790.

[49] C. Xu, A.C. Wang, H. Zou, B. Zhang, C. Zhang, Y. Zi, L. Pan, P. Wang, P. Feng, Z. Lin, Z.L. Wang, Raising the Working Temperature of a Triboelectric Nanogenerator by Quenching Down Electron Thermionic Emission in Contact-Electrification, Advanced Materials, 30 (2018) 1803968.
[50] J. Nie, Z. Ren, L. Xu, S. Lin, F. Zhan, X. Chen, Z.L. Wang, Probing Contact-Electrification-Induced Electron and Ion Transfers at a Liquid–Solid Interface, Advanced Materials, 32 (2020) 1905696.
[51] H. Lei, X. Li, J. Wang, Y. Song, G. Tian, M. Huang, D. Wu, DFT and molecular dynamic simulation for the dielectric property analysis of polyimides, Chemical Physics Letters, 786 (2022) 139131.
[52] S. Rajesh, K.P. Murali, H. Jantunen, R. Ratheesh, The effect of filler on the temperature coefficient of the relative permittivity of PTFE/ceramic composites, Physica B: Condensed Matter, 406 (2011) 4312-4316.
[53] J. Wang, C. Wu, Y. Dai, Z. Zhao, A. Wang, T. Zhang, Z.L. Wang, Achieving ultrahigh triboelectric charge density for efficient energy harvesting, Nature Communications, 8 (2017) 88.
[54] J. Wu, X. Wang, J. He, Z. Li, L. Li, Synthesis of fluorinated polyimide towards a transparent triboelectric nanogenerator applied on screen surface, Journal of Materials Chemistry A, 9 (2021) 6583-6590.
[55] I. Professional Plastics Electrical Properties of Plastic Materials. https://www.professionalplastics.com/professionalplastics/ElectricalPropertiesofPlastics.pdf (accessed July, 2022).
[56] J. Zhou, J. Yang, Y. Shen In 3D heterogeneous integration technology using hot via MMIC and silicon interposer with millimeter wave application, 2017 IEEE MTT-S International Microwave Symposium (IMS), 4-9 June 2017; 2017; pp 499-502.
[57] G. Hougham, G. Tesoro, A. Viehbeck, J. Chapple-Sokol, Polarization effects of fluorine on the relative permittivity in polyimides, Macromolecules, 27 (1994) 5964-5971.
[58] G. Kleyman, T. Kang, J. Twiefel, W. Voit, Characterization of triboelectric charge generation between PTFE and nylon after repeated contacts, Energy Harvesting and Systems, 4 (2017) 165-176.

Author introduction

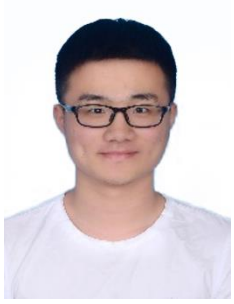

Kaiqiang Wang received his B.S. degree from Dalian University of Technology, China in 2019. Now, he is a Ph.D. student in Department of Mechanical Engineering, Tsinghua University. He was a visiting scholar under the supervision of Prof. Zuankai Wang at the City University of Hong Kong from 2021 to 2022. His current research interest is focused on tribology and solid-liquid triboelectric nanogenerator.

Wanghuai Xu is currently a postdoctoral fellow in the Department of Mechanical Engineering at the City University of Hong Kong. His research interest focuses on water-based energy harvesting, electrical phenomena at the water-solid interface and bioinspired surface engineering.

Jianfeng Li received his B.S. degree in School of Mechanical Engineering, Dalian University of Technology. Now he is a Ph.D. student in Department of Mechanical Engineering, Tsinghua

University. His current research interest is focused on the superlubricity enabled the association effect between two dimensional materials and liquid molecules.

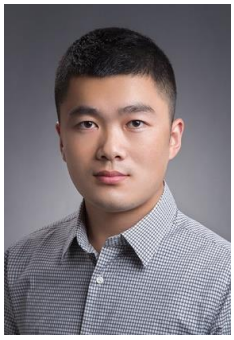

Huanxi Zheng received his M.S. degree at Dalian university of technology in 2017, and Ph.D. degree in City University of Hong Kong in 2020. His research interests mainly focus on bioinspired materials, surface engineering and energy harvesting.

Shouyi Sun received his B.S. degree in engineering mechanics and Ph.D degree in mechanics from Northwestern Polytechnical University, Xi'an, China, in 2014 and 2020, respectively. He worked as a postdoctor at the Department of Mechanical Engineering, Tsinghua University, Beijng, China, from 2021 to 2023. He is currently an associate professor at Northwestern Polytechnical University, Xi'an, China. His current research interests are the solid-liquid synergistic lubrication, the mechanism of superlubricity and the surface strengthening technology.

Wei Song received his Ph.D.degree in Physical Chemistry in 2021 from Sun Yat-sen University, China. He was a visiting Ph.D. student in Tribology Group at Imperial College London, UK, from November 2019 to October 2021. Since January 2022, he started to work as a postdoctoral researcher in the State Key Laboratory of Tribology in Tsinghua University, China. His research interest includes friction modifier (FM) under boundary lubrication.

Yuxin Song is currently a postdoc researcher in Department of Mechanical Engineering at City University of Hong Kong. He obtained his Ph.D. degree under the supervision of Prof. Zuankai Wang at City University of Hong Kong in 2022. His research mainly focuses on lubricant-infused surface and energy harvesting.

Zhengmao Ding received his Ph.D. from Beijing Institute of Technology, China in 2021. Now,

he is an assistant researcher in Department of Mechanical Engineering, Tsinghua University. He was a Postdoc under the supervision of Prof. Jianbin Luo and Jinjin Li at Tsinghua University from 2021 to 2022. His current research interest is focused on 2D materials and osmotic energy generation.

Rui Zhang received his B.S. degree from Shandong University, China, in 2020. He is currently a PhD student in the Department of Mechanical Engineering, Tsinghua University, China. His current research interests are anti-icing/de-icing interface and its mechanism.

Yilin Sun is now an undergraduate student at School of Vehicle and Mobility, Tsinghua University, China. His current research interest is focused on materials science and tribology.

Hanli Zhang received his B.S. and M.S. degree from Tianjin University, China in 2019 and 2022, respectively. His current research interest is focused on solid-liquid triboelectric nanogenerator.

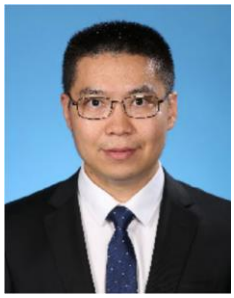

Jinjin Li received the B.S. degree in mechanical engineering from University of Science and Technology of China, Hefei, China, in 2009, and the Ph.D. degree in mechanical engineering from Tsinghua University, Beijing, China in 2014. He is currently an associate professor at Tsinghua University, Beijing, China. His major research area includes solid and liquid superlubricity, nanotribology, friction theory, and solid-liquid triboelectric nanogenerator.

Zuankai Wang is currently chair professor of Nature-Inspired Engineering in the Department of Mechanical Engineering at the Hong Kong Polytechnic University. He serves as the Executive Editor-in-Chief of Droplet journal (Wiley), associate editor and advisory board member for several journals, respectively. His research mainly focuses on Nature-inspired surfaces and materials, additive manufacturing, energy harvesting, fluid dynamics, soft matter, interfaces and surfaces.